Emergence of coherence and the dynamics of quantum phase transitions

Simon Braun[a,b], Mathis Friesdorf[c], Sean S. Hodgman[a,b], Michael Schreiber[a,b], Jens Philipp Ronzheimer[a,b], Arnau Riera[c,d], Marco del Rey[e], Immanuel Bloch[a,b], Jens Eisert[c], and Ulrich Schneider[a,b,1]

[a]Fakultät für Physik, Ludwig-Maximilians-Universität, 80799 Munich, Germany; [b]Max-Planck-Institut für Quantenoptik, 85748 Garching, Germany; [c]Dahlem Center for Complex Quantum Systems, Freie Universität Berlin, 14195 Berlin, Germany; [d]Max-Planck-Institut für Gravitationsphysik, 14476 Potsdam-Golm, Germany; and [e]Instituto de Fisica Fundamental, Consejo Superior de Investigaciones Científicas, 28006 Madrid, Spain

Edited by William D. Phillips, National Institute of Standards and Technology, Gaithersburg, MD, and approved February 9, 2015 (received for review May 19, 2014)

The dynamics of quantum phase transitions pose one of the most challenging problems in modern many-body physics. Here, we study a prototypical example in a clean and well-controlled ultracold atom setup by observing the emergence of coherence when crossing the Mott insulator to superfluid quantum phase transition. In the 1D Bose–Hubbard model, we find perfect agreement between experimental observations and numerical simulations for the resulting coherence length. We, thereby, perform a largely certified analog quantum simulation of this strongly correlated system reaching beyond the regime of free quasiparticles. Experimentally, we additionally explore the emergence of coherence in higher dimensions, where no classical simulations are available, as well as for negative temperatures. For intermediate quench velocities, we observe a power-law behavior of the coherence length, reminiscent of the Kibble–Zurek mechanism. However, we find nonuniversal exponents that cannot be captured by this mechanism or any other known model.

ultracold atoms | optical lattice | Mott insulator | nonequilibrium dynamics | quantum simulation

Phase transitions are ubiquitous but rather intricate phenomena, and it took until the late 19th century until a first theory of classical phase transitions was established. Quantum phase transitions (QPTs) are marked by sudden drastic changes in the nature of the ground state on varying a parameter of the Hamiltonian. They constitute one of the most intriguing frontiers of modern quantum many-body and condensed matter physics (1–4). Although it is typically possible to adiabatically follow the slowly changing ground state in a gapped phase, where the lowest excitation is separated from the ground state by a finite energy, these spectral gaps usually close at a QPT. Because the correlation length simultaneously diverges, adiabaticity is bound to break down, and several important questions emerge. How does a state dynamically evolve across the QPT (i.e., how does the transition literally happen?)? To what extent can the static ground state of a gapless phase be prepared in a realistic finite-time experiment? When entering a critical phase associated with an infinite correlation length, such as superfluid or ferromagnetic order, at what rate and by what mechanism will these correlations build up? Despite the fundamental importance of these questions, satisfactory answers have not been identified so far. Although the intrinsic complexity of the underlying nonintegrable models hinders numerical studies in most cases, the progress in the field of ultracold atoms now enables quantitative experiments in clean, well-isolated, and highly controllable systems.

Here, we study the quantitative dynamics of a transition into a gapless, superfluid phase in the regime of short and intermediate quench times, finding complex behavior outside the scope of any current theoretical model. As a prototypical many-body system with a QPT, we use the transition from a Mott insulator to a superfluid in the Bose–Hubbard model (5–8) by changing (quenching) a parameter of the Hamiltonian. The nonequilibrium settings considered here are relatively well-understood for sudden quenches, where the buildup of superfluid correlations (coherence) can be described by the ballistic spreading of quasiparticles (9, 10). These excitations are generated during the instantaneous parameter change and spread with a group velocity limited by Lieb–Robinson bounds (11). For continuous quenches, the situation is substantially more complex, because the continuous change of the Hamiltonian leads to drastically different elementary excitations throughout the evolution. Moreover, a continuous quench typically starts in the ground state, and the relevant excitations are only created during the ramp. Although there is a large body of literature trying to capture these intricate dynamics of creation and change of quasiparticles in terms of scaling laws (12–14), a comprehensive and fully satisfactory theory is lacking, and many questions are still largely open. These descriptions are built on, for example, adiabatic perturbation theory (3, 15) or scaling collapses (13, 16, 17). Free models allow an exact treatment (18, 19) and can help to build an intuition for more complex physical systems. The Kibble–Zurek framework (12, 20–23) provides a simple guideline for the growth of correlations and predicts the density of defects after asymptotically slow ramps. It is, however, still not satisfactorily understood which correlation length results from crossing a phase transition in a strongly correlated model at a finite rate. The situation is aggravated by the fact that, in 2D and 3D lattice systems, the available numerical techniques do not allow an accurate classical numerical simulation of this setting for long evolution times.

In this work, we use ultracold atoms in an optical lattice to study the Mott to superfluid transition in the Bose–Hubbard model for experimental timescales far away from the adiabatic

Significance

Quantum phase transitions are characterized by a dramatic change of the ground-state behavior; famous examples include the appearance of magnetic order or superconductivity as a function of doping in cuprates. In this work, we explore how a system dynamically crosses such a transition and in particular, investigate in detail how coherence emerges when an initially incoherent Mott insulating system enters the superfluid regime. We present results from an experimental study using ultracold atoms in an optical lattice as well as numerical simulations and find a rich behavior beyond the scope of any existing theory. This quantum simulation of a complex many-body system is an important stepping stone for a deeper understanding of the intricate dynamics of quantum phase transitions.

Author contributions: I.B., J.E., and U.S. designed research; S.B., M.F., S.S.H., M.S., J.P.R., A.R., M.d.R., and J.E. performed research; S.B. and M.F. analyzed data; and S.B., M.F., I.B., J.E., and U.S. wrote the paper.

The authors declare no conflict of interest.

This article is a PNAS Direct Submission.

[1]To whom correspondence should be addressed. Email: ulrich.schneider@lmu.de.

This article contains supporting information online at www.pnas.org/lookup/suppl/doi:10.1073/pnas.1408861112/-/DCSupplemental.

limit. We extract the coherence length from the width of the interference peaks in time-of-flight (TOF) absorption images and observe that, as expected, the final coherence length depends strongly on the quench rate (Fig. 1*A*). Although the resulting coherence length should diverge in the limit of adiabatic ramps, fast quenches result in short coherence lengths. We are able to probe this phase transition experimentally in 1D, 2D, and 3D systems as well as for negative absolute temperature states (24). We compare our measurements in the 1D case with a numerical analysis, finding excellent agreement, and we place them in context with existing theoretical models, thereby uncovering a rich behavior outside the scope of current analytical understanding.

Our experiments (details in *Materials and Methods* and Fig. 1*B*) started by (Fig. 1*B*, I) loading a large Mott insulator of ^{39}K atoms in a 3D optical lattice of depth $V_{\mathrm{lat}} = V_{\mathrm{i}} = 19\ E_{\mathrm{r}}$. Here, $E_{\mathrm{r}} = h^2/(2m\lambda_{\mathrm{lat}}^2)$ denotes the recoil energy with Planck's constant h, the atomic mass m, and the lattice wavelength $\lambda_{\mathrm{lat}} = 736.65$ nm. The onsite interaction energy of the Bose–Hubbard Hamiltonian (24) is denoted by U, and the tunneling matrix element is denoted by J. Because of the strong repulsive interaction of $U/J \geq 250$, the resulting state within the Mott core is close to the atomic limit of a product state with one atom per site. In the deep lattice (Fig. 1*B*, II), the scattering length was then tuned within a wide range of values by a Feshbach resonance at a magnetic field of $B = 402.50\ G$ (25), resulting in different values of the initial interaction strength $(U/J)_{\mathrm{i}}$ in the deep lattice. We have verified numerically that this Feshbach ramp is very close to adiabatic, such that, within the central Mott insulator, the state at this point can be assumed to be the ground state of the system (*SI Appendix*, section G). After this state preparation, the Mott to superfluid phase transition was crossed (Fig. 1*B*, III) by linearly ramping down the lattice depth along the horizontal x direction to $V_{\mathrm{lat}}^{x} = V_{\mathrm{f}} = 6\ E_{\mathrm{r}}$ in variable times t_{ramp} $[V_{\mathrm{lat}}(t) = V_{\mathrm{i}} + (V_{\mathrm{f}} - V_{\mathrm{i}}) \cdot t/t_{\mathrm{ramp}}]$, resulting in a smaller interaction strength $(U/J)_{\mathrm{f}}$ in the final shallow lattice. For experiments in 2D and 3D, we simultaneously ramped down the lattice depth along both horizontal directions or all three directions, respectively. This procedure allows us to control the final interaction strength $(U/J)_{\mathrm{f}}$ by the Feshbach resonance without changing the final lattice ramps and results in a fixed interaction ratio of $(U/J)_{\mathrm{i}}/(U/J)_{\mathrm{f}} \approx (24,\ 35,\ 50)$ (1D, 2D, and 3D). After the ramp, we immediately switched off all trapping potentials and recorded absorption images along the vertical z direction after a TOF of $t_{\mathrm{TOF}} = 7$ ms (Fig. 1*C*). From the width of the interference peaks, we extracted the coherence length of the system (i.e., the characteristic length scale of an assumed exponential decay of correlations) by calculating the expected TOF profiles for various coherence lengths and fitting them to the experimental data (*Materials and Methods* and Fig. 2*A*). We parameterize the ramp time by the dimensionless quantity $\tau_{\mathrm{ramp}} = t_{\mathrm{ramp}} \cdot 2\pi\bar{J}/h \approx t_{\mathrm{ramp}} \cdot 0.93/\mathrm{ms}$, which equals the integrated number of tunneling times $(\tau = h/2\pi J)$ during the ramp. Here, $\bar{J} = \int_{V_{\mathrm{i}}}^{V_{\mathrm{f}}} J(V)\mathrm{d}V/(V_{\mathrm{i}} - V_{\mathrm{f}})$ denotes the average tunneling rate during the ramp. This dimensionless ramp time is directly proportional to the inverse of the quench rate at the critical point (12).

We focus on the short and intermediate ramp time regime, where mass transport is negligible, such that the final density distribution is approximately given by that of the initial Mott insulator, which we take to be one particle per site. Under this assumption, the dynamics are governed by the behavior of the homogeneous system at the multicritical tip of the Mott lobe (5), because a superfluid with unit density connects to the Mott lobe precisely at the tip. Our experiment captures for the first time, to our knowledge, the physics of essentially homogeneous quantum systems entering a gapless, superfluid phase. In contrast, previous work (26) investigated the generic transition through the side of the Mott lobe, which is typical for inhomogeneous systems and dominated by mass transport, and studied the inverse superfluid to Mott insulator transition (27), the vacuum to superfluid transition (28, 29), or the transition of spinor Bose–Einstein condensates to a ferromagnetic state (30).

The experimentally measured coherence length (Fig. 2) displays several distinct dynamical regimes. For very fast ramps, the evolution can be approximated as being sudden, and the measured coherence length-ξ essentially equals that of the initial Mott insulator-ξ_{i}. The latter is significantly below one lattice spacing $d_{\mathrm{lat}} = \lambda_{\mathrm{lat}}/2$ and increases for smaller $(U/J)_{\mathrm{i}}$ closer to the critical point at $(U/J)_{\mathrm{c}} \approx 3.3$ in 1D (31). For larger τ_{ramp}, ξ quickly increases up to several lattice spacings. For $\tau_{\mathrm{ramp}} \gtrsim 2-5$, the fitted ξ starts to decrease again because of the influence of the trap. Contrary to a homogeneous system, the equilibrium distributions of both density and entropy density in a trapped system depend strongly on the interaction strength. Although strong interactions result in a large Mott insulating core with constant density surrounded by a superfluid or thermal shell at lower density, a weakly interacting superfluid is described by a parabolic Thomas–Fermi distribution. Intuitively speaking, the density distribution cannot equilibrate during fast and intermediate lattice ramps and results in gradients in the chemical potential, which give rise to dephasing between lattice sites that increases over time and becomes relevant for slower ramps, $\tau_{\mathrm{ramp}} \gtrsim 2-5$ (*SI Appendix*, section D). Furthermore, although entropy in an ideal bosonic Mott insulator is located predominantly in the surrounding noninsulating shell, it is distributed more homogeneously in a superfluid. Thus, for short times, the trapped system is indistinguishable from the homogeneous

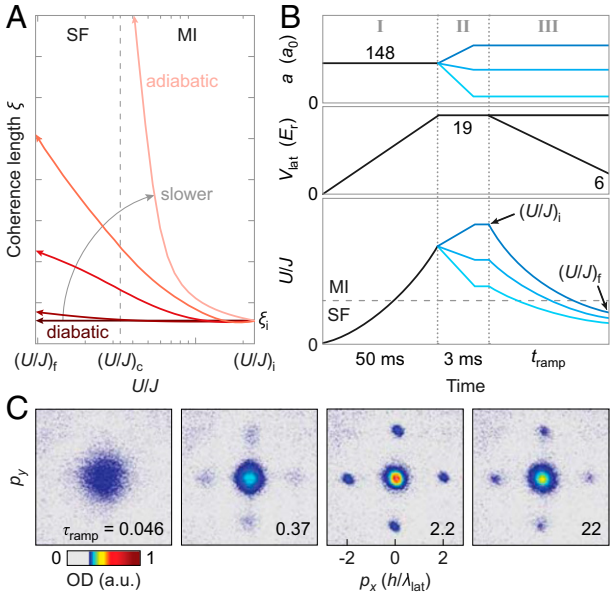

Fig. 1. Growth of coherence length during a quench and experimental sequence. (*A*) Numerical calculation of the evolution of the coherence length-ξ when ramping from a strong interaction $(U/J)_{\mathrm{i}}$ in the Mott insulating (MI) regime over the critical point $(U/J)_{\mathrm{c}}$ to $(U/J)_{\mathrm{f}}$ in the superfluid (SF) regime in a homogeneous 1D system. The colors indicate the quench velocity, from fast (dark red) to the infinitely slow adiabatic limit (light red). (*B*) Experimental sequence for scattering length a (in units of the Bohr radius a_0), lattice depth V_{lat}, and U/J. During I, we prepare a large central Mott insulator with unity filling. The different scattering length values a chosen in II lead to different initial $(U/J)_{\mathrm{i}}$ and final $(U/J)_{\mathrm{f}}$ values for the final lattice ramp in III performed in variable time t_{ramp}. In 1D, only one lattice direction is reduced in the final lattice ramp. In 2D, only two lattice directions are reduced in the final lattice ramp. The horizontal dashed line indicates the critical $(U/J)_{\mathrm{c}}$, separating the SF from the MI regime. (*C*) Recorded TOF absorption images for $(U/J)_{\mathrm{f}} = 3.2$ [$(U/J)_{\mathrm{i}} = 110$] in 2D for several τ_{ramp} (in the text).

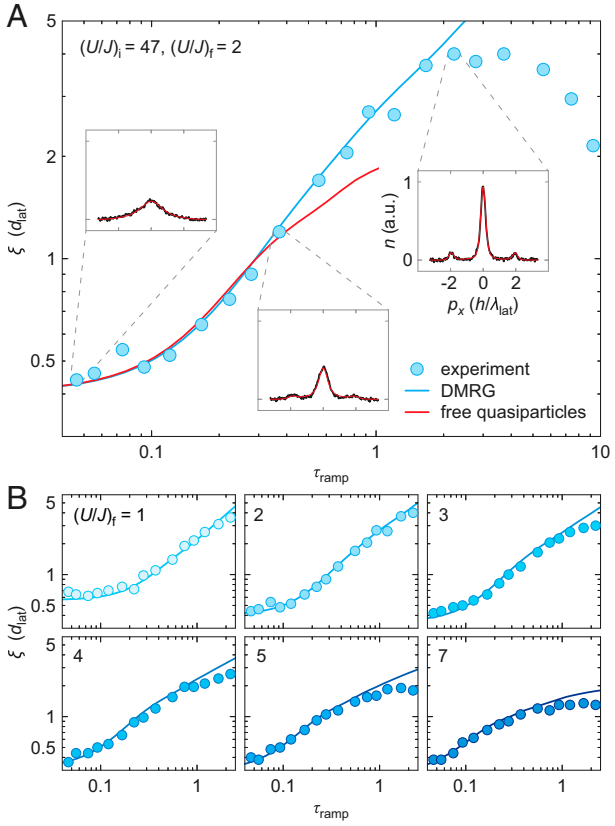

Fig. 2. Emergence of coherence for increasing ramp times. *A*, *Insets* show integrated absorption images (black) for the 1D sequence with corresponding fits of a modeled interference pattern (red) (*Materials and Methods*). The resulting coherence lengths-ξ are shown in *A* vs. τ_{ramp} in a double-logarithmic plot. The blue curve shows a density matrix renormalization group (DMRG) calculation, and the red curve shows the doublon–holon free quasiparticle model (*SI Appendix*, section F). (*B*) ξ vs. τ_{ramp} for several $(U/J)_f$ values in 1D. Points indicate experimental data, and solid curves show DMRG data. Throughout this work, the ramp time is measured in integrated tunneling times (in the text).

system, whereas for longer times, trapping effects dominate the dynamics (32, 33).

The measured emergence of coherence observed here is, indeed, a generic feature of the homogeneous Bose–Hubbard model (i.e., without trap), which can be seen by directly comparing the experimental data with a classical density matrix renormalization group (34) simulation of the homogeneous system based on matrix-product states (Fig. 2*B*) (35). The sole input parameters for the simulation were U and J, and no fitting to the experimental data points was performed. By extensive scaling in bond dimension as well as Trotter step size, we have ensured numerical convergence. Additional cross-validation was obtained by an optimized exact diagonalization code performing a Runge–Kutta numerical integration of a homogeneous Bose–Hubbard model on 15 sites (*SI Appendix*, section E). We find excellent agreement between experiment and numerical data for small and intermediate ramp times up to $\tau_{ramp} \approx 1$. For larger τ_{ramp}, the coherence length of the simulated homogeneous system continues to increase, whereas the experimental data start to decrease because of the trap.

In the fast and slow quench limits, the physics of the continuous quench in the homogeneous model can be understood from two complementary viewpoints. For fast ramps, $\tau_{ramp} \lesssim 0.2$, the dynamics can be well-described in terms of ballistically spreading quasiparticles implemented in a doublon–holon fermionic model (Fig. 2*A* and *SI Appendix*, section F). In this picture, fermionic excitations are continuously created during the quench and spread with their corresponding velocity that can be shown to follow a Lieb–Robinson bound (11, 36–41). For intermediate ramps, $\tau_{ramp} \gtrsim 0.2$, interactions between the quasiparticles become important. For slow ramps, however, one can use the language of adiabatic quenches and the adiabatic theorem. In the beginning of the ramps, the gap is sufficiently large, and we can expect the system to perfectly follow the change of the ground state. Closer to the phase transition, this approximation breaks down, and the full complexity of the problem emerges. If the breakdown of the adiabatic approximation occurs sufficiently close to the critical point, where the physics are governed by scaling laws, the Kibble–Zurek mechanism suggests a power-law growth of the correlation length, where the exponent is governed by the critical exponents of the QPT (22, 23).

We find that, also in our setting, the evolution can be captured in terms of simple power laws (Fig. 3). Within a range of τ_{ramp} of around one order of magnitude, the growth of the coherence length is very well-approximated by a power law:

$$\xi(\tau_{ramp}) = a\tau_{ramp}^{b}. \quad [1]$$

This finding is rather surprising, because rough estimates suggest that the above adiabaticity condition is not fulfilled in the intermediate ramp time regime studied in this work. By using fits to the

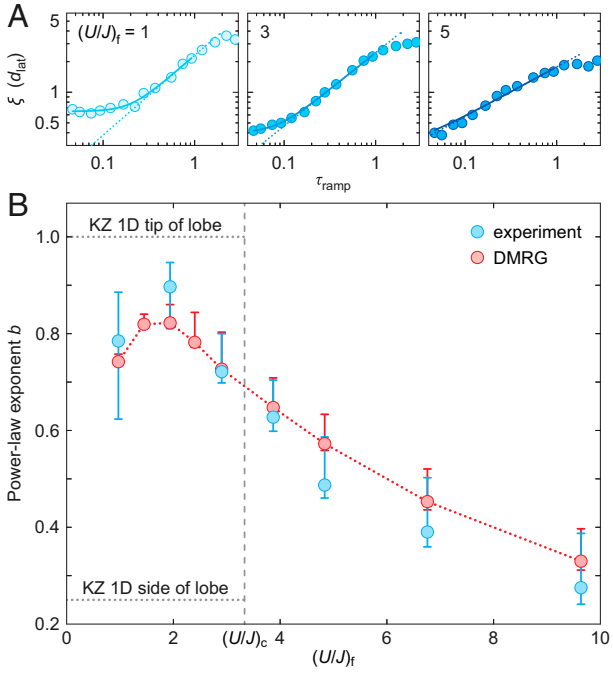

Fig. 3. Power-law increase of coherence length. (*A*) Power-law fits to experimental data in 1D. The fit function $\xi(\tau_{ramp}) = (\xi_i^4 + (a\tau_{ramp}^b)^4)^{1/4}$ heuristically includes the initial coherence ξ_i and is applied to all ramp times up to $\tau_{ramp}^{max} = 1.0$. Here, a, b, and ξ_i serve as free fit parameters, except for $(U/J)_f > (U/J)_c$, where ξ_i is fixed to numerically calculated values (*SI Appendix*, section C). The dotted lines show the pure power-law $\xi(\tau_{ramp}) = a\tau_{ramp}^b$ for the above fitted parameters. (*B*) Exponents b for experiment (blue) and density matrix renormalization group (DMRG; red) extracted by identical fitting procedures. The error bars include the effect of various fitting ranges as well as the fitting uncertainties (*SI Appendix*, section C). The red dotted line guides the eye. The vertical dashed line indicates the critical value $(U/J)_c \approx 3.3$ for the Mott superfluid transition, and the horizontal dotted lines indicate the predictions $b = 1$ and $b = 1/4$ (42) of a typical Kibble–Zurek (KZ) model at the tip or side of the Mott lobe, respectively (in the text and *SI Appendix*, section G).

PHYSICS

experimental or numerical data, we extract the exponent b (Fig. 3), finding values that are always substantially lower than $b = 1$, which was suggested by earlier theoretical works based on the Kibble–Zurek mechanism for the transition at the tip of the Mott lobe (43); however, the used dimensionless ramp time yields the same exponents as the commonly used inverse quench rate at the critical point (12). Although in principle, the resulting exponents may be influenced by the precise ramp timing (*SI Appendix*, section G), the quenches are well-approximated by linear ramps in a large range around the phase transition (*SI Appendix*, section A). More refined studies of this 1D transition, which is of the Kosterlitz–Thouless type, show that, for realistic experimental scales, smaller power laws are expected (44). Our main finding on the dynamics of the 1D phase transition, however, cannot be captured by a simple scaling model. The observed exponent crucially depends on the final point $(U/J)_\mathrm{f}$ of the quench.

In the experiment, ramps with different final values $(U/J)_\mathrm{f}$ also have different initial interactions $(U/J)_\mathrm{i}$ but follow the same ramp scheme $(U/J)(t) = (U/J)_\mathrm{i} \cdot u(t)$ (Fig. 1*B*), where $u(t)$ depends only on the dimension (*SI Appendix*, section A). Because the first part of the evolution is, however, essentially adiabatic, changing the starting point of the ramp does not significantly alter the emerging scaling laws (*SI Appendix*, section G). Because of the rather small resulting coherence lengths, we can also rule out finite-size effects as the origin for the $(U/J)_\mathrm{f}$ dependence of the exponents, which was further corroborated by numerical simulations on systems of various sizes (*SI Appendix*, section E). The simulations also show that the inhomogeneous density cannot be the reason for the $(U/J)_\mathrm{f}$ dependence, because the homogeneous model considered in the numeric, the experimental data agree extremely well, and the influence of the trap is only visible for ramp times $\tau_\mathrm{ramp} \gtrsim 1$ (*SI Appendix*, section D). An inhomogeneous Kibble–Zurek scaling has recently been analyzed for a classical phase transition in ion chains (45, 46) and QPTs (26) as well as thermal (47, 48) phase transitions in ultracold atom systems. In contrast, the agreement between the inhomogeneous experiment and the numerics for the homogeneous system together with the fact that there is no mass transport on these timescales (*SI Appendix*, section B) clearly show that we effectively probe the multicritical QPT of the homogeneous Bose–Hubbard model not influenced by trap effects.

Fig. 4 shows the results of analogous experiments for the 2D and 3D Bose–Hubbard model, which are inaccessible to analytical models as well as current numerical tools. After having verified that the observed quantum dynamics in 1D, indeed, agree with the homogeneous Bose–Hubbard model, the experiments in 2D and 3D can be regarded as analog quantum simulations in a regime out of reach of classical simulation using known methods. Interestingly, the data for higher dimensions show similar power laws as the 1D case, although any critical scaling analysis would strongly depend on dimensionality. Thus, we again find that the dynamics of the Mott to superfluid phase transition on the studied intermediate timescale show complex behavior, which simple approaches based on the critical exponents alone, such as the Kibble-Zurek mechanism, cannot fully capture.

Although the extracted exponents, for the most part, increase for decreasing interaction strength, they start to decrease again for $(U/J)_\mathrm{f} \lesssim 2$ in all dimensions (Fig. 4*B*). Furthermore, the full coherence dynamics for $\tau_\mathrm{ramp} \lesssim 1$ seem to be almost independent of dimensionality and are mainly governed by the final interaction $(U/J)_\mathrm{f}$. Therefore, in the regime where ξ has increased only up to a few d_lat, the influence of dimensionality on the spreading of correlations is marginal. Higher-dimensional systems continue the power-law behavior for longer ramp times than in lower dimensions. This deviation might be explained by the different critical values $(U/J)_\mathrm{c}$ in 1D, 2D, and 3D. For the same final $(U/J)_\mathrm{f}$ value, the quench in the 1D system ends closer to or even deeper in the Mott regime than for higher dimensions,

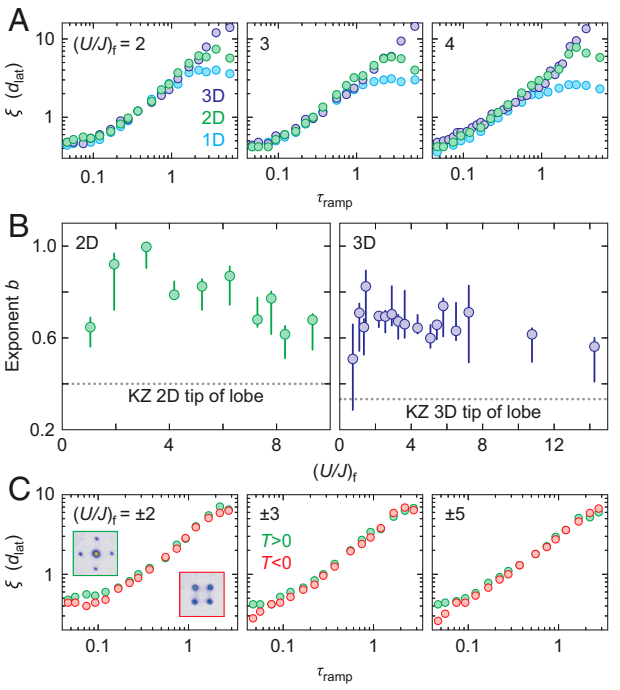

Fig. 4. Emergence of coherence in higher dimensions and for negative absolute temperature. (*A*) Experimental data for 1D, 2D, and 3D for various $(U/J)_\mathrm{f}$. (*B*) Exponents for the 2D and 3D cases extracted from power-law fits to the experimental data with the identical fitting procedure as in Fig. 3. The dotted lines indicate the Kibble–Zurek (KZ) predictions $b = 0.4$ and $b = 1/3$ for the tip of the Mott lobes in the 2D and 3D cases, respectively. (*C*) Experimental data for the 2D case for positive and negative absolute temperature for various $(U/J)_\mathrm{f}$. *Insets* in *Left* show TOF images for both cases at $\tau_\mathrm{ramp} = 2.2$.

limiting the maximum achievable coherence length in addition to the dephasing effect in the trap. A rigorous comparison between different dimensions would have to involve a detailed analysis of the ramp schemes as well as the different mass flow predictions and the individual critical values together with the different scaling of the equilibrium correlations (i.e., quasilong-range order in 1D vs. true long-range order in higher dimensions).

To show that the timescale for the emergence of coherence is not influenced by any possible remnant phase order in the initial state that might seed the dynamics, we additionally studied the emergence of coherence in the attractive Bose–Hubbard model. By crossing the Feshbach resonance and additionally, inverting the external confinement in the deep lattice (II in Fig. 1*B*), we can realize an attractive Mott insulator at negative absolute temperature (24, 49–51) (*SI Appendix*, section G). In Fig. 4*C*, we compare the emergence of coherence between attractive and repulsive interactions in 2D and find essentially identical behavior. Deviations from this symmetric behavior appear only for stronger interactions and can most likely be attributed to multiband effects (52, 53). Because positive and negative temperature superfluids occupy completely different quasimomenta with different correlations (Fig. 4*C*, *Insets*), we conclude that the emergence of coherence observed in the experiment is truly governed by the generic behavior of the continuous quench.

In conclusion, by performing an experimental quantum simulation, we have studied the emergence of coherence across a QPT for various interactions, dimensionalities, and positive and negative absolute temperatures. In 1D, we have also performed a detailed theoretical and numerical analysis and found very good agreement between experiment and density matrix renormalization group calculations. The observed dynamics go beyond the regime of free quasiparticles, and despite its complexity,

we find that a simple power-law growth emerges in a regime where neither the adiabatic theorem nor Lieb–Robinson bounds can characterize the evolution. Although this power law is reminiscent of a Kibble–Zurek type scaling, we find that, in the studied intermediate ramp time regime, the exponent depends on $(U/J)_f$ and depends much less on dimensionality than suggested by the Kibble–Zurek mechanism.

Our findings go beyond current theoretical models and raise the question of how well the dynamical features of a QPT in complex models can generally be captured in terms of simple scaling laws by either systematically expanding the free quasiparticle picture or starting from the Kibble–Zurek mechanism. The success of the latter for slow quenches in a variety of specific models suggests that, compared with a full solution of the model, much less knowledge may be sufficient to characterize the evolution. A satisfactory answer to this question will be crucial for a theory of the dynamics of QPTs. Because exact numerical techniques are not available in higher dimensions, this work may inspire a deeper and more systematic analysis of the computational power of analog quantum simulators in general. For example, it seems timely to identify, in the language of complexity theory, the precise way in which quantum simulators are, indeed, more powerful, even in the absence of error correction, than their classical analogs and how accurately experimental quantum simulators can ultimately be certified as functioning quantum devices.

Materials and Methods

The experiments started with essentially pure condensates of, depending on dataset, $(25-85)\cdot 10^3$ bosonic ^{39}K atoms in an oblate dipole trap with trap frequencies of $\omega = 2\pi\cdot(50, 50, 181)$ Hz along the (x, y, z) direction. We linearly ramped up a 3D optical lattice to a depth of $V_{lat} = 19\ E_r$ (I in Fig. 1*B*). In the 1D case, we then quickly increased the transverse lattice depth to $V^y_{lat} = V^z_{lat} = 30\ E_r$ to minimize correlations along the y and z directions. The scattering length during this loading procedure was $a = 148\ a_0$, resulting in $(U/J)_x \approx 350$ (1D) or $U/J \approx 270$ (2D and 3D; i.e., deep in the Mott insulating regime close to the atomic limit). The trap frequency was increased during the loading to $(94, 94, 159)$Hz in the 1D and 2D cases and $(78, 78, 227)$Hz in the 3D case to ensure a large Mott insulating region in the center of the cloud.

The momentum distribution of the atoms in the optical lattice typically probed using absorption imaging after long TOF is given in refs. 54 and 55:

$$\langle \hat{n}(\mathbf{k})\rangle = \frac{1}{\mathcal{N}}|\tilde{w}(\mathbf{k})|^2 S(\mathbf{k}), \quad [2]$$

with the Fourier transform of the onsite Wannier function $\tilde{w}(\mathbf{k})$ determining the overall envelope of the interference pattern and a normalization factor $\mathcal{N}$. The interference term $S(\mathbf{k})$ has the form of a discrete Fourier transform and is given by a sum over all lattice sites at positions $\mathbf{r}_\mu$ and $\mathbf{r}_\nu$,

$$S(\mathbf{k}) = \sum_{\mathbf{r}_\mu,\mathbf{r}_\nu} e^{i\mathbf{k}(\mathbf{r}_\mu-\mathbf{r}_\nu)}\langle \hat{a}^\dagger_\mu \hat{a}_\nu\rangle, \quad [3]$$

where $\hat{a}^\dagger_\mu$ and $\hat{a}_\mu$ are the creation and annihilation operators, respectively, for a boson on site μ.

In the experiment, we probe the momentum distribution using a finite TOF $t_{TOF} = 7$ ms and attribute a momentum $\mathbf{k} = m\mathbf{r}_{TOF}/(\hbar t_{TOF})$ to each position $\mathbf{r}_{TOF}$ in real space. Because of the finite TOF, the initial density distribution still influences this measured distribution, and the interference term is generalized to (54)

$$\tilde{S}(\mathbf{k}) = \sum_{\mathbf{r}_\mu,\mathbf{r}_\nu} e^{i\mathbf{k}(\mathbf{r}_\mu-\mathbf{r}_\nu)-i\frac{m}{2\hbar t_{TOF}}(\mathbf{r}_\mu^2-\mathbf{r}_\nu^2)}\langle \hat{a}^\dagger_\mu \hat{a}_\nu\rangle. \quad [4]$$

The second term in the exponential provides a correction to a pure Fourier transform and is equivalent to the quadratic term in the Fresnel approximation of near-field optics. We model the correlators by assuming exponentially decaying correlations between lattice sites:

$$\langle \hat{a}^\dagger_\mu \hat{a}_\nu\rangle_{(T>0)} = \sqrt{n_\mu}\cdot\sqrt{n_\nu}\cdot\exp\left(-\frac{|\mathbf{r}_\mu-\mathbf{r}_\nu|}{\xi}\right). \quad [5]$$

Here, ξ denotes the coherence length, and n_μ is the density at site μ. Because different tubes are uncorrelated in the 1D case, off-diagonal elements only contribute if $\mathbf{r}_\mu$ and $\mathbf{r}_\nu$ are within the same tube. As a consequence, we can perform the summation of Eq. **4** for individual tubes and then, integrate the result over all tubes. Because the density distribution is approximately constant over the range of the coherence length-ξ, we can change the order of summations and for every position along a tube, first integrate the densities over all tubes. These doubly integrated densities then enter into Eq. **5**, and by approximating them by a Gaussian distribution of width R, we finally arrive at (*SI Appendix*, section B)

$$\langle \hat{a}^\dagger_\mu \hat{a}_\nu\rangle_{(T>0)} = \exp\left(-\frac{\mathbf{r}_\mu^2+\mathbf{r}_\nu^2}{4R^2}-\frac{|\mathbf{r}_\mu-\mathbf{r}_\nu|}{\xi}\right). \quad [6]$$

In the case of negative temperatures, the correlator contains an additional phase term,

$$\langle \hat{a}^\dagger_\mu \hat{a}_\nu\rangle_{(T<0)} = \langle \hat{a}^\dagger_\mu \hat{a}_\nu\rangle_{(T>0)}\cdot e^{i(\mathbf{r}_\mu-\mathbf{r}_\nu)\cdot 2\pi/\lambda_{lat}}, \quad [7]$$

where $\boldsymbol{\pi} = (\pi, \pi, \pi)$.

To extract the coherence length in the system, we integrate the TOF images over a small region of width $d_{int} \approx 0.2ht_{TOF}/\lambda_{lat}m$ along the y direction. We fit the resulting interference pattern with calculated patterns of the above model for various-ξ and fixed R and extract the coherence length-ξ from the fit (*SI Appendix*, section A). We determine R independently by fitting a Gaussian distribution to in situ images (*SI Appendix*, section B). Sample fits are shown in Fig. 2*A*, *Insets* for the 1D case. Although this rather simple ansatz cannot reproduce the numerically calculated correlation functions in detail (*SI Appendix*, section E), it is sufficient to reproduce the experimentally measured interference patterns. Extracted coherence lengths are shown in Fig. 2*A*. In the case of the 2D and 3D sequences, correlations also spread in the transverse directions. To extract the coherence length, we integrate the images in the same range of diameter d_{int} along the y direction as for 1D and fit the calculated 1D interference patterns to the resulting data.

ACKNOWLEDGMENTS. We thank Marc Cheneau, Masud Haque, Corinna Kollath, Michael Kolodrubetz, Alessandro Silva, Christian Gogolin, Lode Pollet, and Wojciech H. Zurek for discussions; Salvatore Manmana for insights into numerical aspects; and Tim Rom for assistance in setting up the experiment. We acknowledge financial support by Deutsche Forschungsgemeinschaft Grant FOR801 (Deutsch-Israelisches Kooperationsprojekt Quantum Phases of Ultracold Atoms in Optical Lattices), the US Defense Advanced Research Projects Agency (Optical Lattice Emulator Program), Nanosystems Initiative Munich, Spanish Ministerio de Economía y Competitividad Project FIS2011-29287, the Spanish Junta para la Ampliación de Estudios Predoctoral Program, CAM Research Consortium QUITEMAD S2009-ESP-1594, the European Union (Simulations and Interfaces with Quantum Systems), the European Research Council (Taming nonequilibrium quantum systems), Studienstiftung des Deutschen Volkes.

1. Sachdev S (1999) *Quantum Phase Transitions* (Cambridge Univ Press, Cambridge, United Kingdom).
2. (2008) Focus issue on quantum phase transitions. *Nat Phys* 4(3):157–204.
3. Polkovnikov A, Sengupta K, Silva A, Vengalattore M (2011) Nonequilibrium dynamics of closed interacting quantum systems. *Rev Mod Phys* 83(3):863–883.
4. Vojta T (2003) Disorder-induced rounding of certain quantum phase transitions. *Phys Rev Lett* 90(10):107202.
5. Fisher MPA, Weichman PB, Grinstein G, Fisher DS (1989) Boson localization and the superfluid-insulator transition. *Phys Rev B* 40(1):546–570.
6. Jaksch D, Bruder C, Cirac JI, Gardiner CW, Zoller P (1998) Cold bosonic atoms in optical lattices. *Phys Rev Lett* 81(15):3108–3111.
7. Greiner M, Mandel O, Esslinger T, Hänsch TW, Bloch I (2002) Quantum phase transition from a superfluid to a Mott insulator in a gas of ultracold atoms. *Nature* 415(6867):39–44.
8. Bloch I, Dalibard J, Zwerger W (2008) Many-body physics with ultracold gases. *Rev Mod Phys* 80(3):885–964.
9. Cheneau M, et al. (2012) Light-cone-like spreading of correlations in a quantum many-body system. *Nature* 481(7382):484–487.
10. Barmettler P, Poletti D, Cheneau M, Kollath C (2012) Propagation front of correlations in an interacting Bose gas. *Phys Rev A* 85(5):053625.
11. Lieb EH, Robinson DW (1972) The finite group velocity of quantum spin systems. *Commun Math Phys* 28(3):251–257.
12. Dziarmaga J (2010) Dynamics of a quantum phase transition and relaxation to a steady state. *Adv Phys* 59(6):1063–1189.
13. Chandran A, Erez A, Gubser SS, Sondhi SL (2012) Kibble-Zurek problem: Universality and the scaling limit. *Phys Rev B* 86(6):064304.
14. Schützhold R, Uhlmann M, Xu Y, Fischer UR (2006) Sweeping from the superfluid to the Mott phase in the Bose-Hubbard model. *Phys Rev Lett* 97(20):200601.

15. Polkovnikov A (2005) Universal adiabatic dynamics in the vicinity of a quantum critical point. *Phys Rev B* 72(16):161201.
16. Nikoghosyan G, Nigmatullin R, Plenio MB (2013) Universality in the dynamics of second-order phase transitions. arXiv:1311.1543.
17. Kolodrubetz M, Clark BK, Huse DA (2012) Nonequilibrium dynamic critical scaling of the quantum Ising chain. *Phys Rev Lett* 109(1):015701.
18. Cherng RW, Levitov LS (2006) Entropy and correlation functions of a driven quantum spin chain. *Phys Rev A* 73(4):043614.
19. Deng S, Ortiz G, Viola L (2008) Dynamical non-ergodic scaling in continuous finite-order quantum phase transitions. *Eur Phys Lett* 84(6):67008.
20. Zurek WH, Dorner U, Zoller P (2005) Dynamics of a quantum phase transition. *Phys Rev Lett* 95(10):105701.
21. Kibble TWB (1980) Some implications of a cosmological phase transition. *Phys Rep* 67(1):183–199.
22. Zurek WH (1985) Cosmological experiments in superfluid helium? *Nature* 317(6037): 505–508.
23. del Campo A, Zurek WH (2014) Universality of phase transition dynamics: Topological defects from symmetry breaking. *Int J Mod Phys A* 29(08):1430018.
24. Braun S, et al. (2013) Negative absolute temperature for motional degrees of freedom. *Science* 339(6115):52–55.
25. Zaccanti M, et al. (2009) Observation of an Efimov spectrum in an atomic system. *Nat Phys* 5(8):586–591.
26. Chen D, White M, Borries C, DeMarco B (2011) Quantum quench of an atomic Mott insulator. *Phys Rev Lett* 106(23):235304.
27. Bakr WS, et al. (2010) Probing the superfluid-to-Mott insulator transition at the single-atom level. *Science* 329(5991):547–550.
28. Zhang X, Hung CL, Tung SK, Gemelke N, Chin C (2011) Exploring quantum criticality based on ultracold atoms in optical lattices. *New J Phys* 13(4):045011.
29. Zhang X, Hung CL, Tung SK, Chin C (2012) Observation of quantum criticality with ultracold atoms in optical lattices. *Science* 335(6072):1070–1072.
30. Sadler LE, Higbie JM, Leslie SR, Vengalattore M, Stamper-Kurn DM (2006) Spontaneous symmetry breaking in a quenched ferromagnetic spinor Bose-Einstein condensate. *Nature* 443(7109):312–315.
31. Carrasquilla J, Manmana SR, Rigol M (2013) Scaling of the gap, fidelity susceptibility, and Bloch oscillations across the superfluid-to-Mott-insulator transition in the one-dimensional Bose-Hubbard model. *Phys Rev A* 87(4):043606.
32. Bernier JS, Poletti D, Barmettler P, Roux G, Kollath C (2012) Slow quench dynamics of Mott-insulating regions in a trapped Bose gas. *Phys Rev A* 85(3):033641.
33. Natu SS, Hazzard KRA, Mueller EJ (2011) Local versus global equilibration near the bosonic Mott-insulator-superfluid transition. *Phys Rev Lett* 106(12):125301.
34. Schollwöck U (2011) The density-matrix renormalization group in the age of matrix product states. *Ann Phys* 326(1):96–192.
35. Wall ML, Carr LD (2009) *Open Source TEBD*. Available at physics.mines.edu/downloads/software/tebd. Accessed December 2, 2013.
36. Calabrese P, Cardy J (2006) Time dependence of correlation functions following a quantum quench. *Phys Rev Lett* 96(13):136801.
37. Cramer M, Dawson CM, Eisert J, Osborne TJ (2008) Exact relaxation in a class of nonequilibrium quantum lattice systems. *Phys Rev Lett* 100(3):030602.
38. Eisert J, Osborne TJ (2006) General entanglement scaling laws from time evolution. *Phys Rev Lett* 97(15):150404.
39. Bravyi S, Hastings MB, Verstraete F (2006) Lieb-Robinson bounds and the generation of correlations and topological quantum order. *Phys Rev Lett* 97(5):050401.
40. Flesch A, Cramer M, McCulloch IP, Schollwöck U, Eisert J (2008) Probing local relaxation of cold atoms in optical superlattices. *Phys Rev A* 78(3):033608.
41. Läuchli A, Kollath C (2008) Spreading of correlations and entanglement after a quench in the one-dimensional Bose–Hubbard model. *J Stat Mech* 2008(05):P05018.
42. Batrouni GG, Scalettar RT, Zimanyi GT (1990) Quantum critical phenomena in one-dimensional Bose systems. *Phys Rev Lett* 65(14):1765–1768.
43. Cucchietti FM, Damski B, Dziarmaga J, Zurek WH (2007) Dynamics of the Bose-Hubbard model: Transition from a Mott insulator to a superfluid. *Phys Rev A* 75(2):023603.
44. Dziarmaga J, Zurek WH (2014) Quench in 1D Bose-Hubbard model: Topological defects and excitations from Kosterlitz-Thouless phase transition dynamics. *Sci Rep* 4:5950.
45. Ulm S, et al. (2013) Observation of the Kibble-Zurek scaling law for defect formation in ion crystals. *Nat Commun* 4:2290.
46. Pyka K, et al. (2013) Topological defect formation and spontaneous symmetry breaking in ion Coulomb crystals. *Nat Commun* 4:2291.
47. Scherer DR, Weiler CN, Neely TW, Anderson BP (2007) Vortex formation by merging of multiple trapped Bose-Einstein condensates. *Phys Rev Lett* 98(11):110402.
48. Lamporesi G, Donadello S, Serafini S, Dalfovo F, Ferrari G (2013) Spontaneous creation of Kibble-Zurek solitons in a Bose-Einstein condensate. *Nat Phys* 9(10):656–660.
49. Mosk AP (2005) Atomic gases at negative kinetic temperature. *Phys Rev Lett* 95(4): 040403.
50. Rapp A, Mandt S, Rosch A (2010) Equilibration rates and negative absolute temperatures for ultracold atoms in optical lattices. *Phys Rev Lett* 105(22):220405.
51. Mark MJ, et al. (2012) Preparation and spectroscopy of a metastable Mott-insulator state with attractive interactions. *Phys Rev Lett* 108(21):215302.
52. Lühmann DS, Bongs K, Sengstock K, Pfannkuche D (2008) Self-trapping of bosons and fermions in optical lattices. *Phys Rev Lett* 101(5):050402.
53. Best T, et al. (2009) Role of interactions in 87Rb-40K Bose-Fermi mixtures in a 3D optical lattice. *Phys Rev Lett* 102(3):030408.
54. Gerbier F, et al. (2008) Expansion of a quantum gas released from an optical lattice. *Phys Rev Lett* 101(15):155303.
55. Toth E, Rey AM, Blakie PB (2008) Theory of correlations between ultracold bosons released from an optical lattice. *Phys Rev A* 78(1):013627.